PROC. OF JSCE,
No. 238, JUNE, 1975

NUMERICAL ANALYSIS OF THE GROUND WATER MOUND AND FRESH-SALT WATER INTERFACE IN A COASTAL AQUIFER

*By Takeshi KAWATANI**

1. INTRODUCTION

The sea water penetrates more or less into a coastal aquifer. When the ground water table in the aquifer is sufficiently high compared with sea level, the fresh water dischages into the sea and hence the sea-water intrusion can extend little. The increasing demand for ground water in many coastal areas, however, may lower the ground water table. As a result, the seaward flow of fresh water is decreased or even reversed and the sea-water intrusion is allowed to extend far in the aquifer. Several methods have been suggested for controlling or preventing the sea-water intrusion[1]. In order to find the effective applications of those methods and to realize their limitations, many analytical models have been proposed for studying the behavior of sea-water intrusion with respect to the difference between the ground water table and sea level[2]. Some of them treated the effects of the infiltration of rainfall on preventing the intrusion. They have given better understandings about the length of intrusion, the shape of fresh-salt water interface and the amount of fresh-water discharge into the sea. However, it should be remarked that most of these analytical models were studied under steady condition. The problems related to the behavior of sea-water intrusion are mostly unsteady ones. Namely, if the sea-water intrusion responds quickly to the change in fresh water flow, steady solutions may provide good approximations to the shape change of fresh-salt water interface at any moment. In reality, any change in the fresh water flow causes the sea-water intrusion to move slowly toward its new equilibrium position. Thus, the study of the intrusion under unsteady condition becomes important especially when the changes in the fresh water flow are recurred.

This paper reports numerical solutions for the changes in the ground water table and fresh-salt water interface in a coastal aquifer which are induced by a local accretion through the phreatic surface. The mathematical statement of this phenomenon consists of two nonlinear differential equations which are related to each other by the boundary condition on the interface. To describe the unsteady behaviors of the water table and interface, two differential equations should be solved "simultaneously". Exact analytical solutions for these differential equations are not yet possible. One difficulty is due to their nonlinearity and the other is owing to the unsteady condition involved in the problem. Beside trying to find exact analytical solutions, the experiments may be performed by employing the sand box model or viscous flow analog to observe the phenomenon in a coastal aquifer. In this case, the difficulties obviously come out of the scalings of length and time, especially when the research subjects involve the accretion through the phreatic surface. Therefore, the numerical study may be a worthy approach to realize the overall behavior of the unsteady phenomenon in a coastal aquifer. In this work, the explicit finite difference method[3] is employed to solve two "simultaneous" differential equations, expecting that its applicability may be examined through the investigation of numerical solutions for the problem studied herein. The results clarify the unsteady behaviors of ground water table and interface due to a local replenishment, and prove the applicability of the numerical method. It is also noticed that the unsteady condition could not be replaced by the steady condition except when it is done with great care. The numerical results show good qualitative agreement with the experimental results.

2. MODEL FOR NUMERICAL ANALYSIS

The analytical model studied herein is present-

* Ph. D., Associate Professor, Kobe Univ., Kobe.

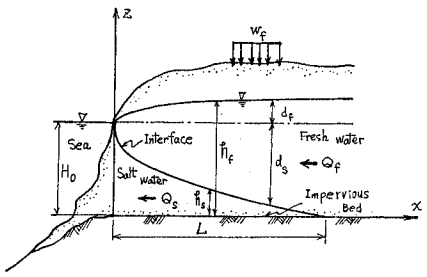

Fig. 1 Analytical model and notations.

ed in Fig. 1 in which coordinates system and notation are also shown. A pervious stratum lies on a horizontal impervious bed. The x-axis coincides with the horizontal bottom of the pervious stratum and the z-axis (vertical axis) goes through the seepage point at the coast. The ground water table in the aquifer is assumed to be a little above sea level so that the sea water penetrates deeply into the pervious stratum. For analytical purposes, the following assumptions are employed; (1) ground water flow is two dimensional and unconfined, (2) pervious stratum is homogeneous and isotropic, (3) mixing of the fresh water and salt water at their boundary is negligible, i.e., the interface between fresh and salt water is clearly identified, (4) vertical velocity component is negligibly small compared with horizontal one except in the vicinity of the coast. That is, the Dupuit approximation can be applied to the flow domain considered herein, (5) hydraulic conductivity of sea water is equal to that of fresh water.

The initial distribution of fresh-salt water interface is supposed to be describable by the Ghyben-Herzberg relationship when the distribution of ground water table is known. In other words, it is assumed that there exists a hydrostatic equilibrium between the two fluids of different densities. The Ghyben-Herzberg relationship is written by

$$d_s=\frac{\rho_f}{\rho_s-\rho_f}d_f \quad \cdots\cdots(1)$$

where as shown in Fig. 1, d_s stands for the depth of fresh-salt water interface below sea level and d_f for the height of free surface above sea level. Moreover, the densities of fresh and salt water are denoted by ρ_f and ρ_s, respectively. In general, $\rho_s=1.025\,\mathrm{g/cm^3}$ and $\rho_f=1.000\,\mathrm{g/cm^3}$. Then, Eq. (1) reduces to

$$d_s=40d_f\,. \quad \cdots\cdots(2)$$

The following is a derivation of differential equations describing the changes in the ground water table and the interface due to a local accretion through the phreatic surface. With the notation shown in Fig. 1, the continuity equations for the region $x\leqq L$ (where L designates the length of the intrusion) are written as, for fresh water regime

$$n\frac{\partial}{\partial t}(h_f-h_s)=\frac{\partial Q_f}{\partial x}+w_f \quad \cdots\cdots(3)$$

and for salt water region

$$n\frac{\partial h_s}{\partial t}=\frac{\partial Q_s}{\partial x} \quad \cdots\cdots(4)$$

where n denotes the porosity of the pervious stratum, and w_f stands for the accretion. The total fresh water and salt water discharges (denoted by Q_f and Q_s, respectively) are taken positive toward the sea. Applying the Dupuit assumption to each fluid separately, the discharges Q_f and Q_s are expressed by

$$Q_f=K(h_f-h_s)\frac{\partial\varphi_f}{\partial x} \quad \cdots\cdots(5)$$

and

$$Q_s=Kh_s\frac{\partial\varphi_s}{\partial x} \quad \cdots\cdots(6)$$

where K designates the hydraulic conductivity and $\varphi_f=z+p/\rho_f g$ is the fresh water potential while $\varphi_s=z+p/\rho_s g$ is the salt water potential (p stands for the pressure at any point in the flow domain and g for the acceleration of gravity). The boundary condition on the fresh-salt water interface is given by[4]

$$H_0-h_s=\frac{\rho_f}{\Delta\rho}\varphi_f-\frac{\rho_s}{\Delta\rho}\varphi_s$$

or differentiating terms on both sides with respect to x

$$\frac{\partial\varphi_s}{\partial x}=\frac{\rho_f}{\rho_s}\frac{\partial\varphi_f}{\partial x}+\frac{\Delta\rho}{\rho_s}\frac{\partial h_s}{\partial x} \quad \cdots\cdots(7)$$

where $\Delta\rho=\rho_s-\rho_f$. Since the Dupuit assumption is employed in this derivation, the fresh water potential is identical with the ground water table, i.e., $\varphi_f=h_f$. Replacing φ_f with h_f, substitution of Eqs. (6) and (7) into Eq. (4) leads to

$$n\frac{\partial h_s}{\partial t}=K\frac{\partial}{\partial x}\left[h_s\left(\frac{\rho_f}{\rho_s}\frac{\partial h_f}{\partial x}+\frac{\Delta\rho}{\rho_s}\frac{\partial h_s}{\partial x}\right)\right] \quad \cdots\cdots(8)$$

On the other hand, substituting Eq. (5) into Eq. (3), the latter becomes

$$n\frac{\partial h_f}{\partial t}-n\frac{\partial h_s}{\partial t}=K\frac{\partial}{\partial x}\left[(h_f-h_s)\frac{\partial h_f}{\partial x}\right]+w_f \quad \cdots\cdots(9)$$

Hence, to find the shapes of free surface and interface at any moment, Eqs. (8) and (9) should be solved simultaneously.

3. NUMERICAL ANALYSIS

It is necessary to eliminate the term of $n(\partial h_s/\partial t)$ from Eq. (9) in order to solve Eqs. (8) and (9) simultaneously by means of a numerical method. Hence, substituting Eq. (8) into Eq. (9), the latter is written by

$$n\frac{\partial h_f}{\partial t}=K\frac{\partial}{\partial x}\left[(h_f-h_s)\frac{\partial h_f}{\partial x}\right]+K\frac{\partial}{\partial x}\left[h_s\left(\frac{\rho_f}{\rho_s}\frac{\partial h_f}{\partial x}+\frac{\Delta\rho}{\rho_s}\frac{\partial h_s}{\partial x}\right)\right]+w_f \quad \cdots\cdots(10)$$

To obtain the numerical solutions for the differential equations, they should be transformed to algebraic finite difference equations. For this purpose, further differentiation is carried out on each term in Eqs. (8) and (10). Thus, they may be rewritten as

$$\frac{n}{K}\frac{\partial h_f}{\partial t}=h_f\frac{\partial^2 h_f}{\partial x^2}+\left(\frac{\partial h_f}{\partial x}\right)^2-\frac{\Delta\rho}{\rho_s}\left[h_s\frac{\partial^2 h_f}{\partial x^2}+\frac{\partial h_s}{\partial x}\frac{\partial h_f}{\partial x}-h_s\frac{\partial^2 h_s}{\partial x^2}-\left(\frac{\partial h_s}{\partial x}\right)^2\right]+\frac{w_f}{K} \quad \cdots\cdots(11)$$

and

$$\frac{n}{K}\frac{\partial h_s}{\partial t}=\frac{\rho_f}{\rho_s}\left[h_s\frac{\partial^2 h_f}{\partial x^2}+\left(\frac{\partial h_f}{\partial x}\right)\left(\frac{\partial h_s}{\partial x}\right)\right]+\frac{\Delta\rho}{\rho_s}\left[h_s\frac{\partial^2 h_s}{\partial x^2}+\left(\frac{\partial h_s}{\partial x}\right)^2\right] \quad \cdots\cdots(12)$$

To obtain nondimensional forms of Eqs. (11) and (12), let

$$X=x/L,\quad H=h_f/L,\quad h=h_s/L \quad \text{and} \quad T=t/(nL/K)$$

where L is the length of the sea-water intrusion. Then, both equations become

$$\frac{\partial H}{\partial T}=\left(H-\frac{\Delta\rho}{\rho_s}h\right)\frac{\partial^2 H}{\partial X^2}+\frac{\Delta\rho}{\rho_s}h\frac{\partial^2 h}{\partial X^2}+\left(\frac{\partial H}{\partial X}\right)^2+\frac{\Delta\rho}{\rho_s}\frac{\partial h}{\partial X}\left(\frac{\partial h}{\partial X}-\frac{\partial H}{\partial X}\right)+\frac{w_f}{K} \quad \cdots\cdots(13)$$

and

$$\frac{\partial h}{\partial T}=\frac{\rho_f}{\rho_s}\left[h\frac{\partial^2 H}{\partial X^2}+\frac{\partial H}{\partial X}\frac{\partial h}{\partial X}\right]+\frac{\Delta\rho}{\rho_s}\left[h\frac{\partial^2 h}{\partial X^2}+\left(\frac{\partial h}{\partial X}\right)^2\right] \quad \cdots\cdots(14)$$

The dimensionless heights H and h are functions of the independent variables X and T. When the X-T plane is subdivided into sets of equal rectangles of sides ΔX and ΔT, the coordinates (X, T) of the representative mesh point P are $X=i\ (\Delta X)$ and $T=j\ (\Delta T)$ as shown in Fig. 2 where i and j are integers. Let denote the values of H and h at P by

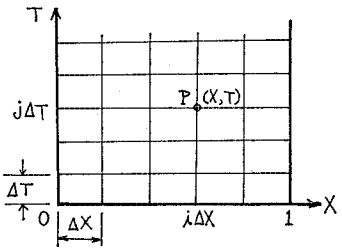

Fig. 2 Coordinates for numerical analysis.

$$H=H(i\Delta X, j\Delta T)=H_{i,j}$$

and

$$h=h(i\Delta X, j\Delta T)=h_{i,j}$$

Then, the explicit finite difference representation of Eqs. (13) and (14) are

$$\frac{H_{i,j+1}-H_{i,j}}{\Delta T}=\left[H_{i,j}-\frac{\Delta\rho}{\rho_s}h_{i,j}\right]\left[\frac{H_{i+1,j}-2H_{i,j}+H_{i-1,j}}{(\Delta X)^2}\right]+\frac{\Delta\rho}{\rho_s}h_{i,j}\left[\frac{h_{i+1,j}-2h_{i,j}+h_{i-1,j}}{(\Delta X)^2}\right]+\left[\frac{H_{i+1,j}-H_{i-1,j}}{2\Delta X}\right]^2+\frac{\Delta\rho}{\rho_s}\left[\frac{h_{i+1,j}-h_{i-1,j}}{2\Delta X}\right]\cdot\left[\frac{h_{i+1,j}-h_{i-1,j}}{2\Delta X}-\frac{H_{i+1,j}-H_{i-1,j}}{2\Delta X}\right]+\frac{w_f}{K} \quad \cdots\cdots(15)$$

and

$$\frac{h_{i,j}-h_{i,j}}{\Delta T}=\frac{\rho_f}{\rho_s}\left[h_{i,j}\left(\frac{H_{i+1,j}-2H_{i,j}+H_{i-1,j}}{(\Delta X)^2}\right)\right]+\frac{\rho_f}{\rho_s}\left[\left(\frac{H_{i+1,j}-H_{i-1,j}}{2\Delta X}\right)\cdot\left(\frac{h_{i+1,j}-h_{i-1,j}}{2\Delta X}\right)\right]+\frac{\Delta\rho}{\rho_s}\left[h_{i,j}\frac{h_{i+1,j}-2h_{i,j}+h_{i-1,j}}{(\Delta X)^2}+\left(\frac{h_{i+1,j}-h_{i-1,j}}{2\Delta X}\right)^2\right] \quad \cdots\cdots(16)$$

Substituting $r=\Delta T/(\Delta X)^2$ into Eqs. (15) and (16), and rearranging both of them,

$$H_{i,j+1}=H_{i,j}+r\left[H_{i,j}-\frac{\Delta\rho}{\rho_s}h_{i,j}\right]\cdot[H_{i+1,j}-2H_{i,j}+H_{i-1,j}]+\frac{\Delta\rho}{\rho_s}rh_{i,j}[h_{i+1,j}-2h_{i,j}+h_{i-1,j}]+\frac{r}{4}[H_{i+1,j}-H_{i-1,j}]^2+\frac{\Delta\rho}{4\rho_s}r[(h_{i+1,j}-h_{i-1,j})^2-(h_{i+1,j}-h_{i-1,j})(H_{i+1,j}-H_{i-1,j})]+\frac{w_f}{K}\Delta T \quad \cdots\cdots(17)$$

and

$$h_{i,j+1}=h_{i,j}+\frac{\rho_f}{\rho_s}r\left[h_{i,j}(H_{i+1,j}-2H_{i,j}+H_{i-1,j})+\frac{1}{4}(H_{i+1,j}-H_{i-1,j})(h_{i+1,j}-h_{i-1,j})\right]+\frac{\Delta\rho}{\rho_s}rh_{i,j}(h_{i+1,j}-2h_{i,j}+h_{i-1,j})+\frac{\Delta\rho}{4\rho_s}r(h_{i+1,j}-h_{i-1,j})^2 \quad \cdots\cdots(18)$$

are obtained.

When the finite difference scheme is applied to the partial differential equation, the unstable growth or stable decay of the errors in the mathematical operations needs to be examined. The explicit finite difference approximation of the linear partial differential equation of parabolic type is stable for[8]

$$r=\Delta T/(\Delta X)^2\leqq 1/2\,.$$

The differential equations treated herein are nonlinear. Although the stability condition for the nonlinear differential equation is not known well, the condition for the linear one is supposed to be applicable in this case. For the numerical computation, the following values are employed;

$L=100$ m (length of the sea-water intrusion)
$K=10^{-3}$ cm/sec (hydraulic conductivity for both fresh and salt water)
$n=0.4$ (porosity)
$\rho_f=1.000$ g/cm^3 (density of fresh water)
$\rho_s=1.025$ g/cm^3 (density of salt water)
$H_0=20$ m (sea level measured from the impervious bed)
$w_f=20$ mm/hr (rate of the local accretion).

If the value of Δx is 2 m (i.e., $\Delta X=2.0\times10^{-2}$), the values of ΔT and Δt satisfying the stability condition stated above are $\Delta T\leqq 2\times10^{-4}$ and $\Delta t=$ 13.3 minutes. Then, the value of $\Delta t=12$ minutes is chosen in this analysis.

It is assumed that the sea-water intrusion is at rest before the accretion begins. In other words, the shapes of the fresh water table and interface are parabolic as expressed by the Ghyben-Herzberg relationship. Thus, the initial shape of free surface is assumed to be given by

$$h_f(x,0)=H_0+0.05\sqrt{x}$$

where x is in meter. This is equivalent to the assumption that the fresh water discharge Q_f is 0.5125 cc/s·m. Then, the initial interface is described by

$$h_s(x,0)=H_0-2.0\sqrt{x}$$

The local accretion through the phreatic surface is supposed to be limited in the region between $x=30$ and 50 m. The length of the intrusion is assumed not to change throughout the analysis. This assumption may be justified as long as the interface displacement is small compared with the thickness of the intrusion. Moreover, the seepage point at the coast and the ground water table just above the end of the intrusion are supposed not to move even if the accretion exists. This situation could be modeled by the situation shown in Fig. 3. Namely, the seepage points coincide with sea level at the coast and fresh water level in the lake.

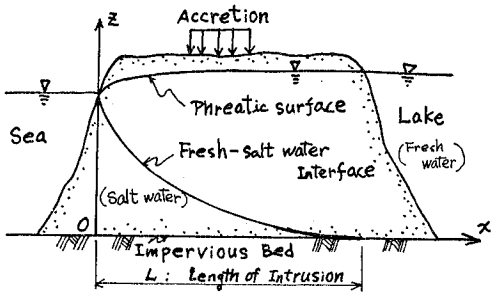

Fig. 3 Model of numerical analysis.

It should be noticed that the numerical results obtained under these assumptions may not correctly describe the water table and the interface near the coast because the vertical velocity component cannot be neglected near the coast and hence the Dupuit approximation is not applicable.

4. RESULTS OF NUMERICAL ANALYSIS AND DISCUSSION

Numerical analysis was carried out for the following two cases; Case I, the local accretion in the region between $x=30$ and 50 m is continued at a constant rate of 20 mm/hr for 12 hours (i.e., from $t=0$ to 12 hrs) and ceased afterwards. The growth and decay of the ground water table (or

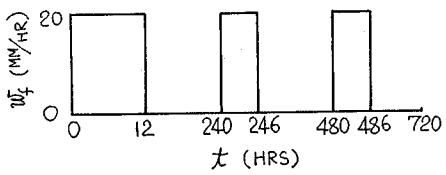

Fig. 4 Model of accretion in Case II.

water mound), and the change in the fresh-salt water interface were computed up to t=1 440 hrs (i.e., 60 days). Case II, the local accretion is repeated three times in this case. The mode of the accretion is displayed in Fig. 4. After the first accretion of 20 mm/hr continues for 12 hours, no accretion holds on until t=240 hrs (or 10 days). Then, the accretion of the same rate for 6 hours is periodically repeated each 10 days. The computation was performed up to t=720 hrs (or 30 days).

The shapes of the ground water table at t=12 and 720 hrs (or 30 days) are shown in Fig. 5 for Cases I and II. The fresh-salt water interface at t=720 hrs are displayed with the initial interface in Fig. 6 for Cases I and II. The water mound grows up to the highest position at t= 12 hrs and spreads afterward in both inland and seaward directions. As mentioned before, the accretion for 6 hours was repeated at t=240 and 480 hrs in Case II, i.e., the total amount of the replenished water in Case II is twice as much as that in Case I. Thus, the ground water table at t=30 days in much higher in Case II than in Case I, and the depressed amount of salt water is much larger in the former case than in the latter. The greatest depressed distance at t=30 days is about 22 cm in Case I while it is approximately 41 cm in Case II. In Figs. 7 and 8, the displacements of the water table from its initial position for Case I are shown in detail. On the other hand, the interface displacements from the

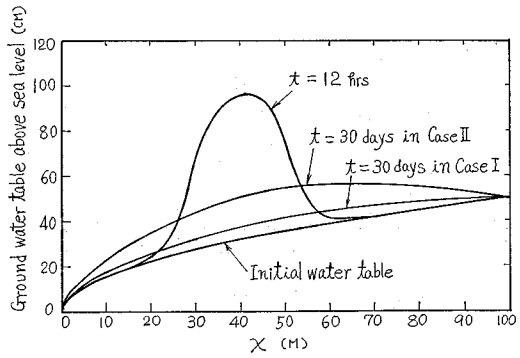

Fig. 5 Ground water tables in Cases I and II.

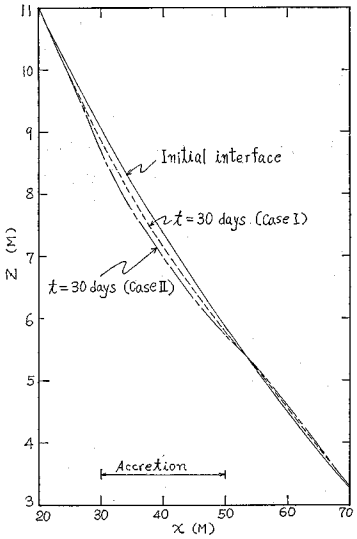

Fig. 6 Fresh-salt water interfaces in Cases I and II.

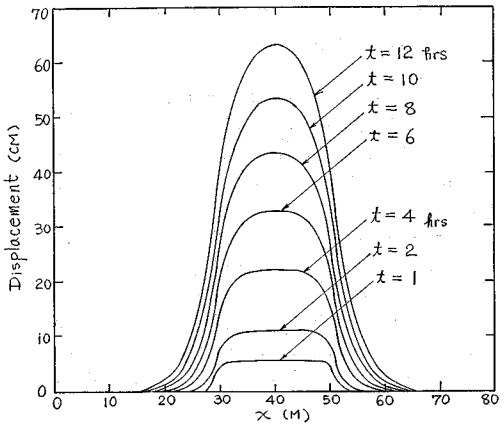

Fig. 7 Displacement of ground water table from the initial position (Case I).

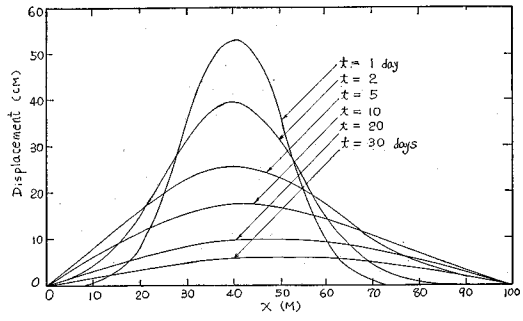

Fig. 8 Displacement of ground water table from the initial position (Case I).

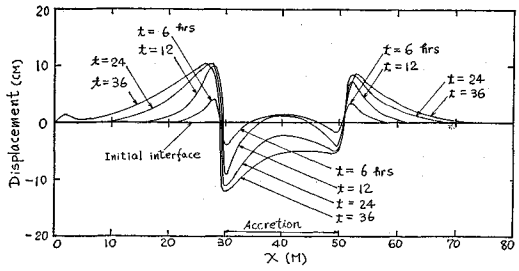

Fig. 9 Displacement of interface from the initial position (Case I).

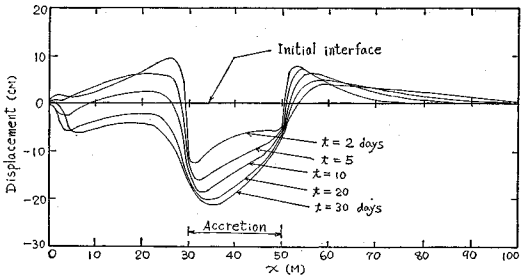

Fig. 10 Displacement of interface from the initial position (Case I).

initial position for Case I are presented in Figs. 9 and 10. The water mound grows up continuously while the local reprenishment proceeds, and the spreading of the mound also goes on. At $t=12$ hrs, the top of the mound rises up to about 60 cm from the initial surface. After the accretion ceases, the mound top descends very slowly and the mound spreads inland and seawards. At $t=720$ hrs, the highest portion of the ground water table is 6 cm above the initial table. On the other hand, when the replenishment is going on, the fresh-salt water interface between $x=30$ and 50 m goes downwards near edges of this region whereas it goes up near the center. The interface starts to rise just outside the replenishment range. This small disturbance in the interface in the early stage of the accretion can be understood as follows. In the early stage, the gradient of the water table is much larger near the edges of the accretion range than near the center. Thus, the fresh water near the edges is expected to move faster than the fresh water near the center. As a result, the salt water close to the edges of the accrtion range is more strongly forced to flow out of the range than the salt water near the center. The salt water flowed out causes the rise of the interface just outside the accretion range.

After the cessation of local replenishment, the

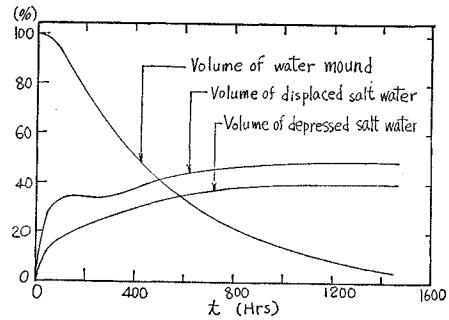

Fig. 11 Temporal changes in the volume of water mound and in the volumes of displaced and depressed salt water (Case I).

interface within the accretion range begins to descend as a whole. Outside the accretion region, although the risen portion of the interface spreads gradually inland and seawards, the top of that portion stops rising and the interface begins to lower as a whole. The descend of the interface is notable in the region between the seaside (or $x=0$ m) and $x=50$ m. Figure 11 is provided to examine the change in the ground water table and interface with time. In this figure, "the volume of water mound" means the volume of fresh water above the initial position normalized by the total volume of replenished water. The volumes of both displaced and depressed salt water are also nondimensionalized by the total volume of replenished water. The volume of ground water mound appears to decrease exponentially with time. This is confirmed in Fig. 12. Namely, the volume of the mound (denoted by V) may be written as

$$V/V_t=\exp(B(t-t_0))$$

where V_t is the total volume of replenished water and t_0 denotes the time when the local accretion

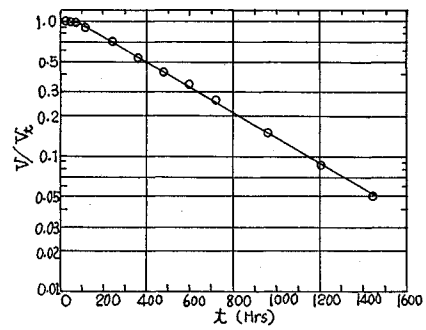

Fig. 12 Temporal change in the volume of water mound (Case I).

begins to alter the initial discharge of fresh water into the sea and the lake, and B is a constant. In this case, the values of t_0 and B are estimated to be 72 hrs (or 3 days) and -0.00205. On the other hand, the fresh-salt water interface is displaced both upwards and downwards during the process of the accretion, i.e., the volume of the displaced salt water increases rapidly during the accretion. However, since the interface begins to descend as a whole after the replenishment stops, the volume of the depressed salt water increases more slowly than the displaced volume. The displaced and depressed volumes become constant at $t=50$ days (or 1 200 hrs). The former volume is about 50% of the total replenished water whereas the latter is about 40%. Moreover, until $t=60$ days (1 440 hrs), the 95% of the replenished amount has discharged. To obtain more information about the shape change of the mound, the displacement of the ground water table from its initial position could be analyzed by regarding it as a "dimensional" probability density function. Thus, it is possible to evaluate the mean value, standard deviation, skewness and flatness factor for the water mound. The results of the evaluation are shown in Fig. 13.

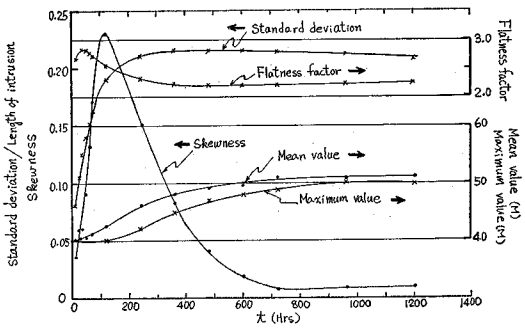

Fig. 13 Shapes of water mound (Case I).

The maximum value (or top of the mound) and mean value of the mound move progressively to $x=0.5$ ($x=50$ m), i.e., the center of the length of the intrusion. This indicates that the shape of the mound tends to be symmetric about $x=50$ m as the mound spreads over the whole length of the intrusion. This tendency is clearly observed in the temporal change in the skewness, too. The asymmetry of the ground water mound about the mean augments rapidly until $t=5$ days (or 120 hrs) and then diminishes gradually as time increases. Although the shape of the mound becomes more symmetric with time, the seaside tail of the mound beyond the standard deviation from the mean is always shorter than the inland tail because the skewness is always positive. The flatness factor tends to be smaller with increasing time until $t=15$ days (360 hrs) and becomes constant afterwards. This is due to the fact that the standard deviation is relatively small until $t=15$ days and hence the volume in both tails of the mound beyond the standard deviation from the mean is large compared with the volume within the standard deviation. Once standard deviation becomes constant, the flatness also becomes constant. Although the results in Fig. 13 give the useful information about the distribution of the ground water table, it is important to notice that the temporal changes of the values in Fig. 13 are subject to the boundary conditions employed in this analysis. That is, since the water table is assumed not to move at $x=0$ and 100 m, all values evaluated above are expected to become constant as time increases.

In order to investigate the effects of the repeated accretions on the growth of ground water mound and on the change in the fresh-salt water interface, the outcomes of the accretions for 6 hours from $t=240$ to 246 hrs and from $t=480$ to 486 hrs were compared with those from $t=0$ to 6 hrs (refer to Fig. 4). The water mounds grown up by the second and third accretions are, as expected, identical in shape (and hence volume) with that by the first accretion of 6 hours. In other words, the ground water tables at $t=246$ and 486 hrs can be obtained by superposing the displacement of the water table from $t=0$ to 6 hrs on the water tables at $t=240$ and 480 hrs, respectively. The displaced volumes of salt water by the first, second and third accretions for 6 hours are also identical with each other. On the other hand, the depressed volumes of salt water by second and third accretions are about 17% larger than that from $t=0$ to 6 hrs. This may indicate that the effect of previous accretions on depressing the interface lasts at least for 10 days while the upward displacement of the interface diminishes rapidly after the cessation of the accretion.

5. EXPERIMENTAL RESULTS

The object of this experiment is to obtain the data which can be used to examine the results of the numerical analysis given above. The experiment was carried out by means of a Hele-Shaw model. The pure glycerine whose specific density is 1.256 was employed as the fresh water. The salt water was modeled by adding sugar to the glycerine. The specific density of the latter

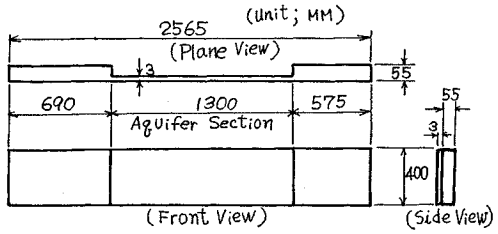

Fig. 14 Experimental equipment and dimensions.

is 1.287. The ratio of these specific densities is 1.025 which coincides with the ratio of the salt-water density to the fresh-water density. On the other hand, the coefficient of the viscosity was measured to be 20.3 poise for the pure glycerine and 43.2 poise for the one added sugar. The former is about one half of the latter. This difference in the viscosity is quite large compared with that in a real flow. The experimental equipment and its dimensions are shown in Fig. 14. The part modeling the aquifer is 130 cm long and 40 cm high. Two parallel plates are 3 mm apart.

The accretion was started after the salt water intrusion extended long enough over the aquifer section. The initial shape of the interface is shown by a dotted line in Fig. 15. In this figure,

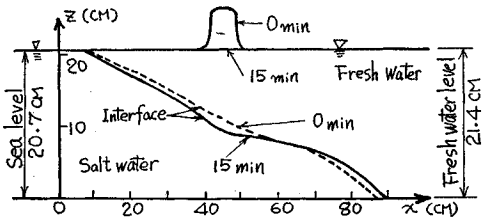

Fig. 15 Water mound and sea-water intrusion (experiment).

the coordinates are also displayed to present the experimental results. The fresh water level was 21.4 cm and sea level was 20.7 cm. As observed in the figure, the length scale of the sea-water intrusion obtained in the experiment is approximately 1/100 of that in the numerical study. Namely, the interface displacement of 23 cm which is the maximum value at $t=30$ days in the numerical analysis corresponds to the displacement of only 0.23 cm in the experimental model. Thus, to have observable displacements of the interface in the experiment, the water mound should be grown up much higher than that in the numerical analysis. In that case, however, the mound was expected to spread extremely wide compared with the mound in the numerical analysis. Therefore, the accretion range in the experiment was shortened to a half of that in the analysis.

The time ratio t_r between the model and the prototype is given by[4] $t_r=t_m/t_p=L_rK(12\nu/b^2g)$, where subscripts m and p stand for model and prototype, respectively. Moreover, L_r is the length ratio, i.e., L_m/L_p, ν is the kinematic viscosity of the fluid used in the experiment, b is the distance between two parallel plates and g is the acceleration of the gravity. For $L_r=1/100$, the phenomena within one minute in the experiment correspond to the phenomena for at most 30 days in the prototype. Hence, it is difficult to observe the phenomena in the early stage of the accretion.

Because of the experimental difficulties mentioned above, it must be pointed out that the results of the numerical study can be examined only "qualitatively" by comparing with the experimental results.

The water mound was formed by pouring the pure glycerine from the top of the aquifer section between $x=40$ and 50 cm. By the reason stated above, the water mound was risen up to the height equal to 1/3 of the ground water depth (whereas the height in the numerical analysis is about 1/30 of the depth). The water mound formed in this way is obviously different from the one in the analysis because the latter spreads when it is growing up. However, the decays of mound in both cases are expected to become similar as time increases.

The shape of the interface at 15 minutes just after the mound began to spread is displayed in Fig. 15 by a solid line. It should be again remarked that the phenomenon within 15 minutes in this experiment is equivalent to the phenomenon within about 450 days in the prototype. As

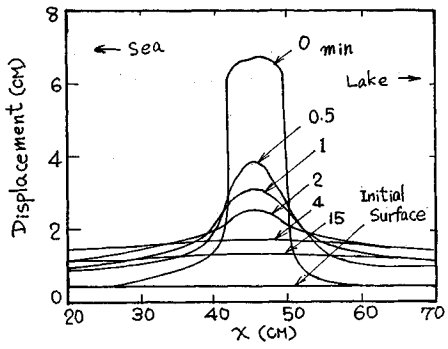

Fig. 16 Decay of water mound (experiment).

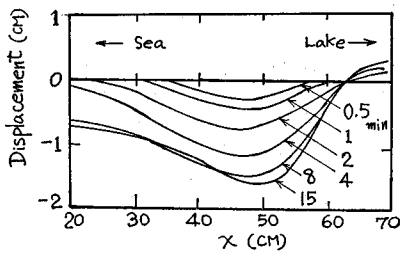

Fig. 17 Displacement of the interface (experiment).

observed in Fig. 15, the interface on the seaward side from the replenishment range is depressed whereas the interface on the inland side is pushed upward. This movement of the interface is very similar to the one shown in Fig. 6. The details of the mound decay are displayed in Fig. 16 and the interface displacement from its initial position is shown in Fig. 17. The depressed interface in the experiment is wider than that in the numerical analysis. This is because the total amount of the replenished water is roughly 5 times as much as the amount in the numerical analysis. Thus, the mound in the experiment spread wider and hence the interface was depressed wider. Nevertheless, it is noticed from these figures that the experimental results are qualitatively similar to those obtained in the analysis. Especially, it is a good agreement with the numerical result that the descent of the interface proceeds continuously in the seaward direction whereas it does not extend farther beyond $x=65$ cm in the inland direction. The rise of the interface outside the replenishment range is less in the experiment than in the numerical analysis. In Figs. 18 and 19, the water mound and the interface displacement are also shown. The above statements are confirmed in these figures, too.

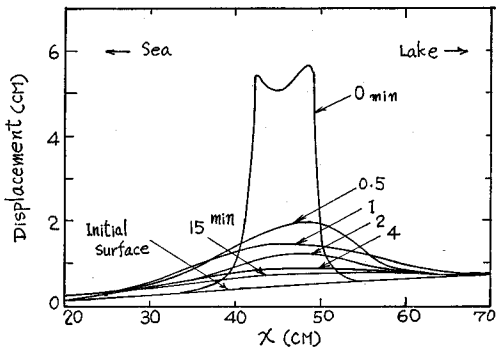

Fig. 18 Decay of water mound (experiment).

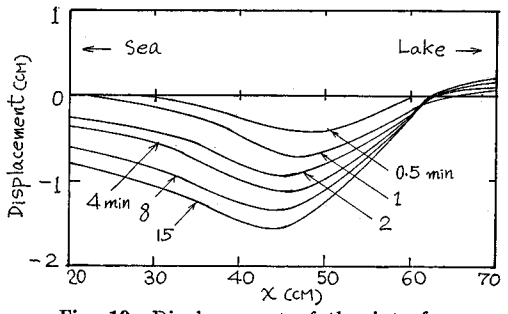

Fig. 19 Displacement of the interface (experiment).

6. CONCLUSION

A numerical analysis was employed to study the unsteady behaviors of the ground-water table and fresh-salt water interface due to a local accretion. The main aims of this analysis were to observe the interaction between two deformable boundaries (i.e., the ground-water table and the interface), and to examine the applicability of the numerical method to similar problems. Since the main attention is directed to the temporal changes of the water table and the interface near the local accretion range, it was assumed that the intrusion length did not change throughout the analysis. Moreover, the interface was assumed to coincide with the ground-water table at the coast. Because of the latter assumption, the Dupuit approximation is no longer applicable near the coast. Therefore, the results obtained in this analysis should be regarded as the behaviors of the phreatic surface and the interface in the relatively early stage of their movements, and should not be extended to the region close to the coast.

The results of the numerical analysis and experiment are summarized as follows;

(1) In the duration of the accretion, the fresh-salt water interface within the accretion range descends gradually near both edges of that range whereas it rises near the center of and just outside the accretion range.

(2) The interface starts to descend from the vicinity of the accretion region as a whole after the accretion ceases. The descent proceeds continuously on the seaward side from the accretion range whereas it extends little on the inland side.

(3) The volume of ground water mound decreases exponentially with time.

(4) The displaced volume of salt water for 50 days is about 50% of the total amount of replenished water and the receded volume of salt water is about 40% of the latter.

(5) The distribution of ground water table due

to repeated accretion could be estimated by superposing the displacement of the table due to previous accretion. The depressed volume of salt water is affected by preceding accretions.

(6) The experimental results obtained in the Hele-Shaw model show good qualitative agreement with the results of the numerical analysis.

ACKNOWLEDGEMENT

The author wishes to express his gratitude to Prof. S. Tanaka for his help and guidance. Special thanks are given to those who assisted in experiment and analysis.

REFERENCES

1) Todd, D. K.: "Ground water hydrology", John Willey & Sons, Inc., 1959.
2) Shima, S.: "Ground water problems related to density current", (Japanese), Text of Summer Seminar on Hydraulic Engineering, 1971.
3) Smith, G. D.: "Numerical solution of partial differential equations", Oxford University Press, 1965.
4) Bear, J.: "Dynamic of fluids in porous media", American Elsevier Inc., 1972.

(*Received Oct. 17, 1974*)